



## LJMU Research Online

**Yan, Z, Raza, N, Van Waerbeke, L, Mead, AJ, McCarthy, IG, Troster, T and Hinshaw, G**

**An analysis of galaxy cluster mis-centring using cosmological hydrodynamic simulations**

<http://researchonline.ljmu.ac.uk/id/eprint/12602/>

### Article

**Citation** (please note it is advisable to refer to the publisher's version if you intend to cite from this work)

**Yan, Z, Raza, N, Van Waerbeke, L, Mead, AJ, McCarthy, IG, Troster, T and Hinshaw, G (2020) An analysis of galaxy cluster mis-centring using cosmological hydrodynamic simulations. Monthly Notices of the Royal Astronomical Society. 493 (1). pp. 1120-1129. ISSN 0035-8711**

LJMU has developed [LJMU Research Online](http://researchonline.ljmu.ac.uk/) for users to access the research output of the University more effectively. Copyright © and Moral Rights for the papers on this site are retained by the individual authors and/or other copyright owners. Users may download and/or print one copy of any article(s) in LJMU Research Online to facilitate their private study or for non-commercial research. You may not engage in further distribution of the material or use it for any profit-making activities or any commercial gain.

The version presented here may differ from the published version or from the version of the record. Please see the repository URL above for details on accessing the published version and note that access may require a subscription.

For more information please contact [researchonline@ljmu.ac.uk](mailto:researchonline@ljmu.ac.uk)

<http://researchonline.ljmu.ac.uk/>

# An analysis of galaxy cluster mis-centring using cosmological hydrodynamic simulations

Z. Yan <sup>1</sup>★, N. Raza, <sup>1</sup>★, L. Van Waerbeke,<sup>1</sup> A. J. Mead,<sup>1,2</sup> I. G. McCarthy <sup>3</sup>,  
T. Tröster <sup>4</sup> and G. Hinshaw<sup>1</sup>

<sup>1</sup>Department of Physics and Astronomy, University of British Columbia, 6224 Agricultural Road, Vancouver, BC V6T 1Z1, Canada

<sup>2</sup>Institut de Ciències del Cosmos, Universitat de Barcelona, Martí Franquès 1, E-08028 Barcelona, Spain

<sup>3</sup>Astrophysics Research Institute, Liverpool John Moores University, 146 Brownlow Hill, Liverpool L3 5RF, UK

<sup>4</sup>Institute for Astronomy, University of Edinburgh, Royal Observatory, Blackford Hill, Edinburgh EH9 3HJ, UK

Accepted 2020 January 28. Received 2020 January 25; in original form 2019 December 13

## ABSTRACT

The location of a galaxy cluster’s centroid is typically derived from observations of the galactic and/or gas component of the cluster, but these typically deviate from the true centre. This can produce bias when observations are combined to study average cluster properties. Using data from the BARYons and HALoes of MAssive Systems (BAHAMAS) cosmological hydrodynamic simulations, we study this bias in both two and three dimensions for 2000 clusters over the  $10^{13}$ – $10^{15}$   $M_{\odot}$  mass range. We quantify and model the offset distributions between observationally motivated centres and the ‘true’ centre of the cluster, which is taken to be the most gravitationally bound particle measured in the simulation. We fit the cumulative distribution function of offsets with an exponential distribution and a Gamma distribution fit well with most of the centroid definitions. The galaxy-based centres can be seen to be divided into a mis-centred group and a well-centred group, with the well-centred group making up about 60 per cent of all the clusters. Gas-based centres are overall less scattered than galaxy-based centres. We also find a cluster-mass dependence of the offset distribution of gas-based centres, with generally larger offsets for smaller mass clusters. We then measure cluster density profiles centred at each choice of the centres and fit them with empirical models. Stacked, mis-centred density profiles fit to the Navarro–Frenk–White dark matter profile and Komatsu–Seljak gas profile show that recovered shape and size parameters can significantly deviate from the true values. For the galaxy-based centres, this can lead to cluster masses being underestimated by up to 10 per cent.

**Key words:** hydrodynamics – methods: numerical – galaxies: clusters: general – galaxies: groups: general – dark matter – large-scale structure of Universe.

## 1 INTRODUCTION

Galaxy clusters are the largest and most massive gravitationally bound systems that we observe today, and as such, form a significant source of information to probe structure formation (Simionescu et al. 2019; Walker et al. 2019) and constrain the cosmological parameters (Mantz et al. 2010; Borgani & Kravtsov 2011). Galaxy clusters are observed across the entire electromagnetic spectrum, and for that reason they also serve as a unique probe of the complex physical processes underlying galaxy formation and evolution. The future landscape of cluster science is very exciting, thanks to the development of new facilities, more sensitive equipment, and better

resolution, allowing large areas of the sky to be surveyed across all wavelengths (Mantz et al. 2019). A key aspect of galaxy cluster science is the construction of cluster catalogues, which involves cluster identification and the measurement of basic features such as size, profile, redshift, morphology, and mass. A crucial element of these measurements that is not often discussed is the definition of cluster centres.

Deconstruction of the cluster weak-lensing signal is a well developed and often used technique that allows us to study these clusters, most notably to recover their mass. However, in the process of this measurement, several assumptions about the shape and structure of the cluster have to be made. One of these is the choice of selecting a centre for the cluster. Traditionally, the definition for the ‘true’ centre of a galaxy cluster is taken to be the deepest point of the gravitational potential well, i.e. where a test particle is most

\* E-mail: [yanza15@phas.ubc.ca](mailto:yanza15@phas.ubc.ca) (ZY); [raza.nayyer@gmail.com](mailto:raza.nayyer@gmail.com) (NR)

bounded to the system. However, calculating this requires knowing the mass distribution for the cluster in at least 2D (and ideally 3D including redshift) in the first place, which is difficult to do using the lensing signal alone. The workaround that has been employed for the past few decades is to use a host of different proxies for the centre that can be directly observed or measured. These proxies are based on our knowledge of the different physical components found in the galaxy cluster itself, such as hot X-ray emitting gas or luminous galaxies, and are theoretically well motivated to trace the true centre. However, as they are fundamentally only approximations to the true cluster centre, our choice for the proxy centre invariably introduces a bias to our measurement of the cluster mass and shape. As the next generation of observing instruments such as the Large Synoptic Survey Telescope (LSST) reach precision capabilities where we can measure the mass to sub-per cent levels, it becomes increasingly important to accurately quantify these centroid-dependent biases and develop a systematic approach to correct for them.

Cluster density profiles are typically measured by stacking profiles from multiple sources, producing a convolution of the true mean profile with the probability distribution function (PDF) of the offset. A model is generally assumed for the PDF of the centroid offsets, and these model parameters are included when fitting (Cibirka et al. 2017). In contrast, with cosmological simulations we know the position of the real centre of each galaxy cluster, thus we can constrain the offset PDF independently of the density measurements. In this study, we use hydrodynamical simulations of galaxy clusters from the BARYons and HALoes of MASSive Systems (BAHAMAS) project (McCarthy et al. 2017) to measure and model the degree of mis-centring in galaxy clusters, and then analyse the effects this has on inferred cluster properties. In using the latest hydrodynamical simulations, we capture the significant effects that baryons have on the structure and formation history of the clusters, as opposed to studying dark matter only gravitational  $N$ -body simulations. Furthermore, as ideal environments where the full 3D distribution of the individual cluster components can be known, the hydrodynamical simulations allow us to exactly compute the various centroids, based on different tracers, for each cluster and compare them with the ‘true’ centres. By studying a large number of clusters ( $\sim 2000$ ) over a diverse mass range ( $10^{13}$ – $10^{15} M_{\odot}$ ), we can capture trends in centroid bias over different cluster shapes and sizes.

These centroid-dependent biases are further explored in the study of the cluster mass density profiles, where empirically established models such as the Navarro–Frenk–White (NFW) dark matter profile (Navarro, Frenk & White 1997) and Komatsu–Seljak (KS) gas profile (Komatsu & Seljak 2001) can be fitted to data. From a theoretical point of view the profile fits inform us of how well current models capture the underlying mass distribution. More importantly, however, from an observational point of view, by performing the stacking of mis-centred profiles from multiple clusters we are able to study how the fitting parameters and related physical properties are affected. This is especially important, since identifying and using consistent centre proxies is essential for accurate stacking of cluster profiles to get high signal-to-noise ratio when analysing real data.

Previous analyses of  $N$ -body simulations, as well as actual lensing data, showed that different centre choices can introduce biases of up to a few per cent [e.g. George et al. 2012; Ford et al. 2015; Schrabback et al. 2018; see also the recent Dark Energy Survey (DES) collaboration study, Zhang et al. 2019]. Cawthon et al. (2018) used the redMaPPer cluster catalogue to characterize mis-centring, and they adopted the X-ray peak position as their reference cluster

centre. We extend their analysis with a larger (simulated) cluster catalogue, more centroid choices, and more offset distribution models.

The paper is organized as follows. In Section 2, we first outline the data used from the BAHAMAS simulations along with the various centroid definitions and their calculations. In Section 3, we then quantify and model the degree of mis-centring. Section 4 follows with analysis of both well-centred and mis-centred density profiles. Key results are summarized in Section 5.

## 2 DATA AND DEFINITIONS

### 2.1 Simulation data

We employ data from the BAHAMAS (McCarthy et al. 2017, 2018) simulations. BAHAMAS is a suite of cosmological, hydrodynamic simulations run using a modified version of the TreePM smoothed particle hydrodynamics (SPH) code GADGET3. The simulations primarily consist of  $400 \text{ cMpc } h^{-1}$  periodic boxes containing  $2 \times 10^{24}$  particles (dark matter and baryonic, in equal numbers). Here we use the run that adopts a *Wilkinson Microwave Anisotropy Probe* (WMAP) 9-year best-fitting cosmology with massless neutrinos (Hinshaw et al. 2013).

BAHAMAS includes subgrid treatments of important physical processes that cannot be directly resolved in the simulations, including metal-dependent radiative cooling, star formation, stellar evolution and mass loss, black hole formation and growth, and stellar and active galactic nuclei (AGN) feedback. The subgrid models were developed as part of the OWLS project (Schaye et al. 2010). The parameters governing the efficiencies of AGN and stellar feedback were adjusted so that the simulations approximately reproduce the observed galaxy stellar mass function for  $M_{*} \geq 10^{10} M_{\odot}$  and the hot gas fraction–halo mass relation of groups and clusters, as determined from high-resolution X-ray observations of local systems. As shown in McCarthy et al. (2017), the simulations match the galaxy–halo–thermal Sunyaev–Zel’dovich (tSZ)–X-ray scaling relations of galaxies and groups and clusters.

For this study, friends-of-friends (FOF) haloes are selected in logarithmic bins of  $M_{200, \text{crit}}$  from a reference dark matter only simulation,<sup>1</sup> which are then matched to the fiducial BAHAMAS hydro simulation. We adopt a bin width of 0.25 dex spanning the range  $10^{13}$ – $10^{15} M_{\odot}$  and randomly select 300 unique haloes per mass bin (or all of the haloes, if there are fewer than 300 in a bin), resulting in a sample of approximately 2000 haloes.

All particles (representing gas, dark matter, and stellar content) in a sphere of radius  $2r_{200}$  centred on the most bound particle (MBP) are selected for analysis. In addition, a galaxy catalogue is produced for all simulated galaxies with  $M_{\text{gal}} > 10^{10} M_{\odot}$  within this radius. Simulated galaxies are defined as the stellar component of self-gravitating substructures identified with the SUBFIND algorithm.

### 2.2 Halo centre definitions

For this study, the halo centre is defined to be the position of the gravitationally most bound particle (MBP), i.e. the halo particle with the minimum gravitational potential. An alternative ‘true centre’ is the point where the total mass density is maximum. As it happens,

<sup>1</sup>We selected haloes from a reference dark matter only simulation, so as to facilitate future comparisons with runs that vary feedback and cosmology.

**Table 1.** The names, abbreviations, and component tracers of the centroids analysed in this study. The most bound particle (MBP) is taken to be the true centre of the galaxy cluster, and the seven other centroids are evaluated with respect to it.

Abbreviation	Full name	Tracer
MBP	Most bound particle	–
SITR	Stars centre from iteration method	Stellar Mass
SMGC	Stars most-massive galaxy centre	Stellar Mass
SMGL	Stars median galaxy location	Stellar Mass
SCOM	Stars centre of mass	Stellar Mass
GSXP	Gas soft X-ray luminosity peak	Soft X-ray
GBXP	Gas bolometric X-ray luminosity peak	Bolometric X-ray
GCYP	Gas Compton $\gamma$ parameter peak	Compton $\gamma$

this coincides with the MBP for most clusters, and since neither this nor the MBP is directly observable, we arbitrarily choose the former as the *true* centre, both in 2D and 3D. We then study the effect that choosing each of seven alternative cluster centre definitions has on the inferred cluster mass and density profile, both in 2D and 3D. These proxy centres are based on different cluster components, which in turn are close to physical cluster observables. The names, definitions, and abbreviations for these centroids are given in Table 1. These proxy centres can be coarsely classified into gas-based or stellar-based tracers.

The gas-based proxies, GSXP, GBXP, and GCYP, are defined as the peak position of the soft X-ray, bolometric X-ray, and Compton  $\gamma$  parameter luminosity, respectively. For each gas particle in the simulations, we have an associated luminosity for each type of emission. To calculate the centroids we first pixelize all the gas particles on to a grid with a pixel/voxel size of  $0.01r_{200}$ , then we smooth the luminosities with a Gaussian beam whose width is equal to the mean gas interparticle distance. The centroids are defined as the centre of the pixel/voxel with the highest luminosity for each of the three observables.

Stellar-based centroids are calculated from the BAHAMAS galaxy catalogue, which is based on stellar mass distributions. The Stars centre from ITerATION method (SITR) is based on a method described in Robotham et al. (2011). For each cluster, we first calculate the centre of stellar mass, then remove the galaxy that is furthest from this centre. In each subsequent iteration, the new centre of stellar mass is found and the furthest galaxy is once again dropped, until there are only two galaxies left. SITR is then taken to be the centre of the more massive galaxy. The Stars Most-massive Galaxy Centre (SMGC) is simply the position of the galaxy with the highest mass inside the cluster halo. The Stars Centre Of Mass (SCOM) is the galaxy-mass-weighted mean position of objects within the halo. The Stars Median Galaxy count Location (SMGL; Andreon 2015) is another iterative scheme. For each cluster, we start with a  $(2r_{200})^3$  volume centred at the SMGC. We count galaxies along each coordinate direction from the origin and find the median position along each axis. We move the centre to the new median position and clip the volume to 0.85 times the previous volume and repeat the search. The iteration ends when the volume dimension reaches  $0.4r_{200}$ . The SMGL is taken to be the position from the last iteration.

For our 2D analysis we generate data from the simulation using the distant-observer approximation, by projecting the positions of all cluster particles on to the plane of the sky. The calculation of each centroid follows the same definition as in 3D. The 2D centres calculated this way more closely resemble real data, while the 3D

centres allow us to utilize the full information available from the simulation.

Fig. 1 shows nine randomly selected clusters from the simulation, with the centroids listed in Table 1 highlighted.

### 3 CHARACTERIZATION OF MIS-CENTRING

#### 3.1 Modelling the offset distribution

The stacked density profile of a group of mis-centred galaxy clusters is typically modelled as an astrophysical profile convolved with a probability distribution function (PDF) of the offset:

$$\rho_{\text{off}}(r|\{q_i, s_j\}) = \int \rho(r_0|\{q_i\})P(r_{\text{off}}|\{s_j\})dr_{\text{off}}, \quad (1)$$

where the centroid offset vector  $\mathbf{r}_{\text{off}}$  is defined as

$$\mathbf{r}_{\text{off}} \equiv \mathbf{r}_{\text{MBP}} - \mathbf{r}_{\text{cen}}, \quad (2)$$

where  $\mathbf{r}_{\text{cen}}$  is one of the centroid positions defined in Table 1 (in 2D or 3D, we use bold type to represent vectors and unbold type to represent their magnitude). In the above,  $\mathbf{r}$  is the position vector with respect to the measured centre, while  $\mathbf{r}_0$  is the position vector relative to the MBP (the true centre):

$$\mathbf{r}_0 \equiv \mathbf{r} - \mathbf{r}_{\text{off}}. \quad (3)$$

The relation among  $\mathbf{r}$ ,  $\mathbf{r}_{\text{off}}$ , and  $\mathbf{r}_0$  is illustrated in Fig. 2.

In equation (1),  $P(r_{\text{off}}|\{s_j\})$  is the PDF model parametrized by  $\{s_j\}$ . So the average profile of mis-centred clusters is described by the density profile parameters  $\{q_i\}$  and the offset PDF model parameters  $\{s_j\}$ . With real data, both  $\{q_i\}$  and  $\{s_j\}$  must be constrained simultaneously (Cibirka et al. 2017). In this paper, we constrain the  $\{s_j\}$  separately, since we know the MBP positions from the simulation.

In this paper, the offsets are measured in units of  $r_{200}$ . Fig. 3 shows the distribution of offsets with respect to  $M_{200}$ . In the figure, we see that the offsets for some of the galaxy-based centroids split into two groups. For these centres, there is one population that effectively tracks the MBP, while the other centres are quite scattered. In order to capture this behaviour, we form a bimodal offset model. Cawthon et al. (2018) find that a combination of an exponential distribution and a Gamma distribution (denoted  $\text{E}\Gamma$  below) is the best model to describe their distribution of centroid offsets. We adopt this model in our analysis, but we consider other parametrizations in Appendix A.

The specific form of the  $\text{E}\Gamma$  model is

$$P_{\text{M}}(r|f, \sigma, \tau) = f \frac{1}{\sigma} \exp\left(-\frac{r}{\sigma}\right) + (1-f) \frac{r}{\tau^2} \exp\left(-\frac{r}{\tau}\right), \quad (4)$$

where  $\sigma$  and  $\tau$  are parameters that describe the width of each population and  $f \in [0, 1]$  is the fraction of clusters that belong to the centred population.

In order to avoid binning artefacts, we fit the model parameters  $f$ ,  $\sigma$ , and  $\tau$  to the cumulative distribution function (CDF) given by

$$C_{\text{M}}(r_{\text{off}}|f, \sigma, \tau) = \int_0^{r_{\text{off}}} P_{\text{M}}(r|f, \sigma, \tau) dr. \quad (5)$$

For each centroid definition, we estimate an empirical  $C_{\text{M}}(r_{\text{off}})$  from the data using all 2000 clusters. We use bootstrap methods to estimate the covariance of each CDF by resampling the clusters 200 times using random draws with replacement. From this ensemble, we calculate the mean  $C_{\text{M}}$  and its covariance, then we fit the

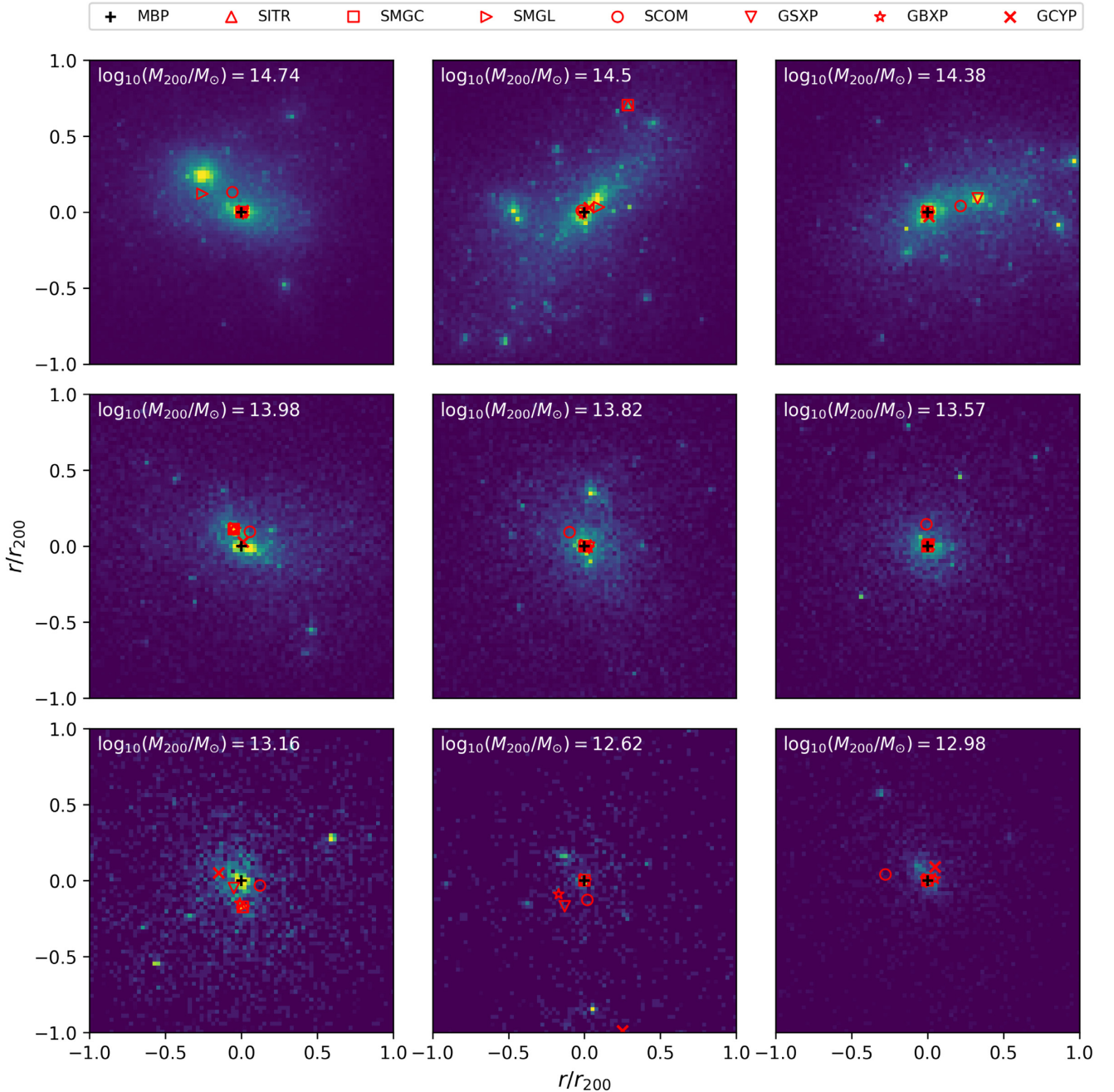


**Figure 1.** Images of nine randomly selected clusters from the simulation colour coded by stellar mass. The projected 3D centroids defined in Table 1 are indicated by the symbols in the legend.

model in equations (A1) and (5). When fitting, we constrain  $\sigma$ ,  $\tau \in [0, 2]$  and  $f \in [0, 1]$ . Fig. 4 shows our sampled CDF estimates along with our model.

The best-fitting  $E\Gamma$  model is compared to the measured CDF in Fig. 4. The measured CDF clearly shows the bimodal behaviour of the SITR, SMGC, and SMGL centroids. Note that  $\sigma$  in these cases is much smaller than  $\tau$  or  $r_{200}$ , which means that the first group, defined by the exponential distribution, is the well-centred group. This group comprises roughly 60 per cent of the clusters. The SITR centroid has a slightly higher well-centred fraction, which means that the iteration method rules out some massive galaxies that are

not physically part of the cluster. For the well-centred group, the most massive galaxy is at the minimum of the gravitational potential of its host cluster.

For the stars centre of mass and gas-based centroids (SCOM, GSXP, GBXP, and GCYP), it is inappropriate to interpret the distribution in terms of a well-centred and mis-centred group because the distributions are clearly not bimodal. In these cases, the exponential and Gamma distributions are simply parametrizing one underlying distribution with additional degrees of freedom. In most cases, however, one model dominates over the other, as measured by the fraction,  $f$ .

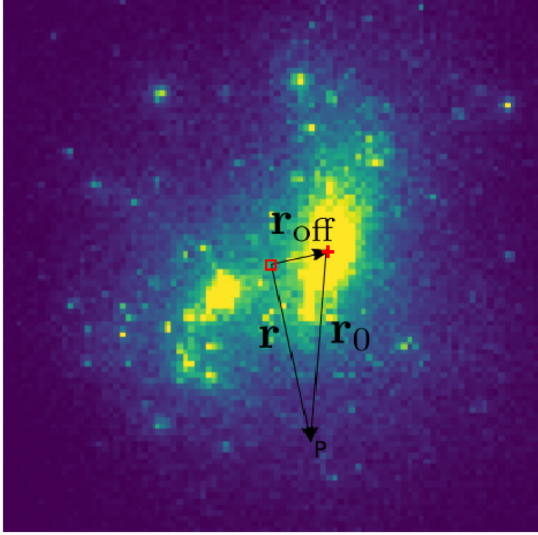


**Figure 2.** An example illustrating the relation among  $r$ ,  $r_{\text{off}}$ , and  $r_0$ .  $P$  is the point where the density profile is measured. The red square is the centroid and red cross is the MBP.

In summary, our results are mixed. When considering all clusters, the gas-based centroids have a smaller scatter than the galaxy-based ones, but the latter centroids significantly outperform the former in roughly 60 per cent of the clusters. Unfortunately, it is difficult to distinguish whether a given cluster is well-centred or mis-centred from the available data. We are currently investigating whether new tools, such as machine learning algorithms, might be of use in addressing this question. Amongst the galaxy-based centroids, the iterative SISTR definition has the highest well-centred fraction and the lowest PDF width, while amongst the gas-based centroids, the X-ray-based ones produce slightly smaller overall scatter than the Compton  $y$ .

We repeated the above analysis with several different PDF parametrizations (see Appendix A) and concluded that the EF model is adequate to parametrize the PDF of the centroid offset distribution. This conclusion agrees with Cawthon et al. (2018).

### 3.2 Mass dependence of the offsets

We next examine the mass dependence of the various centroid offsets. To do so, we segregate the clusters into 15 mass bins of width 0.13 dex, from  $M_{200} = 10^{13}$  to  $10^{15} M_{\odot}$ , and then compute the mean offset for each centroid in each mass bin. The results for our 3D analysis are shown in Fig. 5; the 2D results are qualitatively similar.

The results show that the galaxy-based centroids SISTR, SMGC, and SMGL generally have larger mean offsets than the gas-based centroids. The SCOM offsets hover around  $0.3 r_{200}$  until a cluster mass of about  $10^{14} M_{\odot}$ , above which they steadily decrease with mass. This may occur because the more massive clusters contain a larger number of galaxies with  $M_{\text{gal}} > 10^{10} M_{\odot}$ , which may reduce the shot noise due to outlying massive galaxies that are far from the MBP. The gas-based centroid offsets exhibit a more systematic decrease with cluster mass until  $\sim 10^{14.4} M_{\odot}$ , above which they start to increase. This latter effect may be due to high-mass clusters being more likely to have undergone a major merger in the past, and therefore to have more gas substructure their haloes (Mihos 2003).

## 4 MASS DENSITY PROFILES

Mass density profiles provide valuable information about the size and structure of a galaxy cluster. However, it is usually necessary to average multiple cluster profiles together to gain high signal-to-noise ratio. In doing so, the chosen cluster centre becomes important, as mis-centring produces biased profiles that lead to biased inferences of their physical properties (George et al. 2012). Our aim here is to investigate and quantify this bias as a function of centroid definition.

There are two ways of stacking profiles from cluster observations. One is called the ‘observer point of view’, in which cluster profiles with a similar mass are first stacked and averaged, then the average profile is fit to a model. The other is called the ‘theorist point of view’, in which each cluster profile is individually fit to a model, without stacking, after which the fit parameters are averaged. Since the latter approach requires high signal-to-noise ratio data on individual clusters, we do not explore it further in this paper, choosing instead to characterize the ‘observer point of view’.

### 4.1 Methods and definitions

In this section, we generate average mass density profiles (in 2D and 3D) as a function of cluster mass for each of the centroid definitions presented in Table 1. The clusters are grouped into 10 mass bins of 0.2 dex each, in the range  $10^{13}$ – $10^{15} M_{\odot}$ , and the profiles are binned in units of  $r_{200}$ , defined with respect to the MBP. For diagnostic purposes, we generate density profiles including *all* particles in a cluster, and profiles that includes only gas particles (see below for details). In all, we produce 32 density profiles for each cluster (8 centroid definitions  $\times$  2D or 3D  $\times$  gas or all particles) before forming the average profiles.

To form a density profile, we group a cluster’s particles into 20 equal log-spaced radial bins in the range  $0.1 r_{200} < r < r_{200}$  according to the particle’s distance to the chosen centroid. The bin size and spacing provide a reasonable balance between resolving profile structure and minimizing shot noise within each bin. The 3D profile is measured by summing the masses of particles within each bin and dividing by the bin volume,

$$\rho(\bar{r}_i) = \frac{\sum_a M_a}{\frac{4\pi}{3} (r_{i+1}^3 - r_i^3)}. \quad (6)$$

Here,  $r_i$  is the inner edge of the  $i$ th bin,  $\bar{r}_i \equiv (r_i + r_{i+1})/2$  is the bin centre, and  $M_a$  is the mass of  $a$ th particle within the  $i$ th radial bin. Note that the sum on  $a$  will either include *all* particles in the bin, or only the gas particles.

The 2D profile is defined similarly, except that  $r$  is a projected distance, and the denominator is the bin area,

$$\Sigma(\bar{r}_i) = \frac{\sum_a M_a}{\pi (r_{i+1}^2 - r_i^2)}. \quad (7)$$

Once these profiles are in hand for each cluster and configuration, we average the  $\sim 200$  cluster profiles in each mass bin, and calculate the bin–bin covariance matrix. We then fit the stacked profiles with empirical models from literature, as detailed below.

We model the ‘all-particle’ density profiles with the NFW model, based on dark matter only  $N$ -body simulations (Navarro et al. 1997). This form is commonly used to describe cluster density profiles (see e.g. Łokas & Mamon 2001),

$$\rho_{\text{NFW}}(r) = \frac{\rho_0}{\frac{r}{R_s} \left(1 + \frac{r}{R_s}\right)^2}, \quad (8)$$

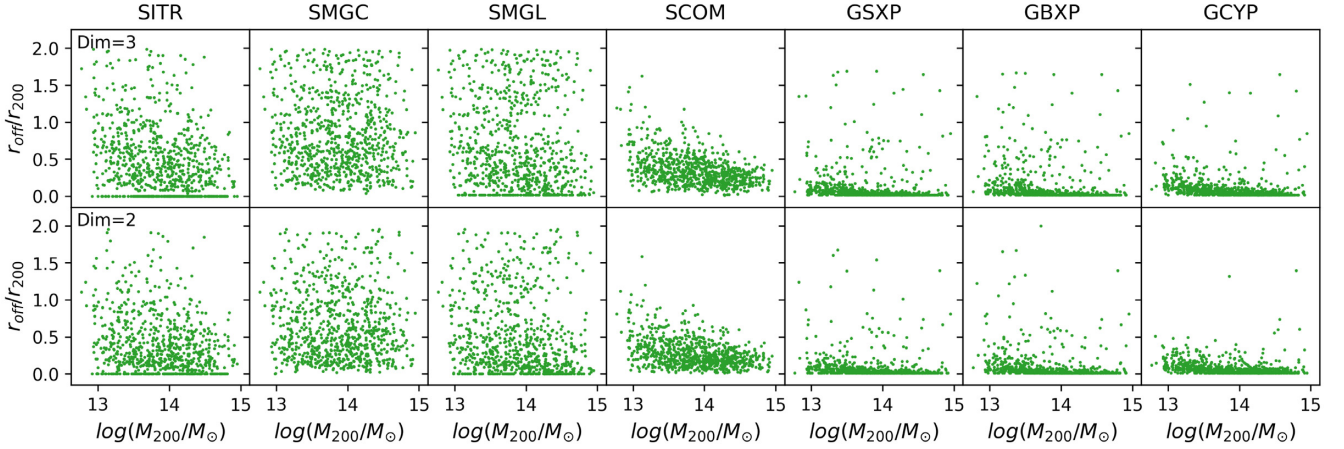


**Figure 3.** Centroid offsets with respect to the MBP as a function of cluster mass,  $M_{200}$ , for each centroid defined in Table 1. The upper panels show results for the 3D centroids, the lower panels for the 2D centroids. For the first three galaxy-based centroids, a significant fraction of the clusters have centroids that coincide with the MBP, while the rest show significantly higher scatter than the gas-based centroids possess.

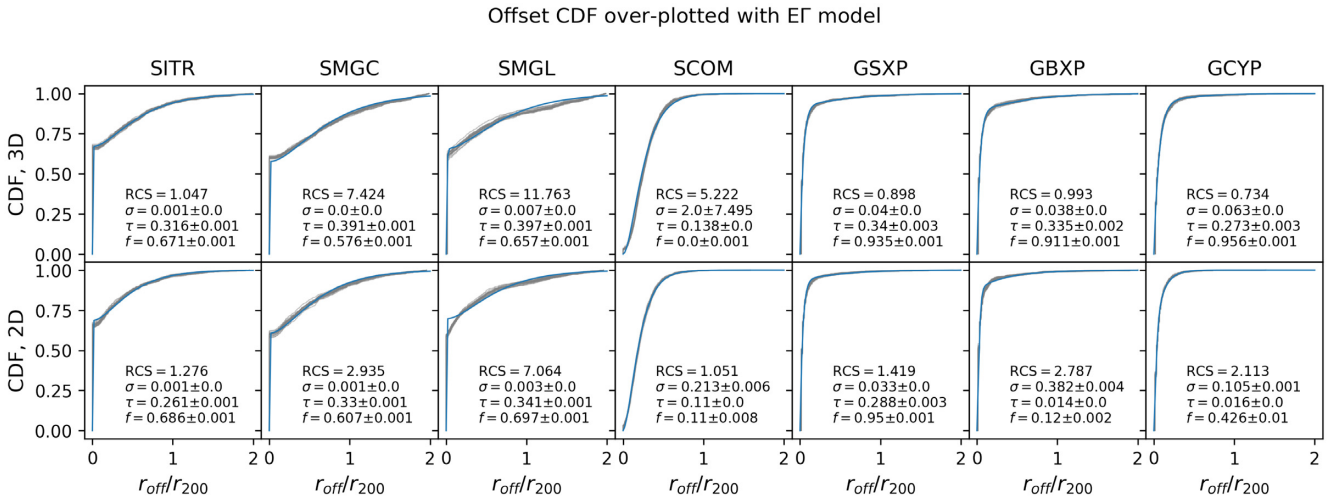


**Figure 4.** The measured (grey) offset CDFs for all the seven centroid definitions, along with their corresponding best-fitting EF model distributions. The best-fitting model parameters and reduced  $\chi^2$  (RCS) values are indicated in each panel. Upper panels: 3D offsets; lower panels: 2D offsets.

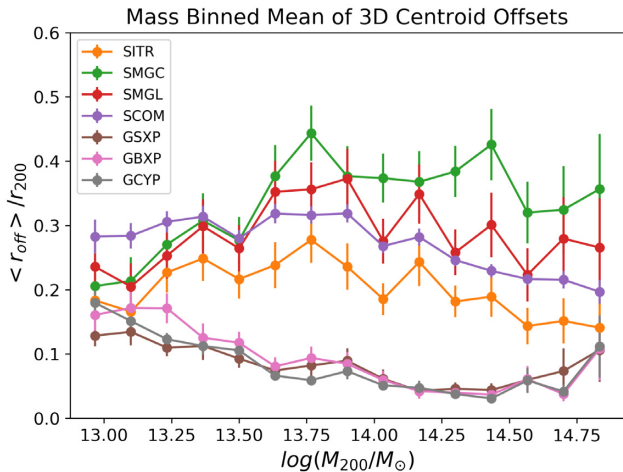


**Figure 5.** The mean 3D centroid offset as a function of cluster mass for each centroid definition. The clusters are binned by their value of  $M_{200}$  between  $10^{13}$  and  $10^{15} M_{\odot}$ . The plotted uncertainty is the standard deviation of the centroid offset in each mass bin. The 2D results are qualitatively similar.

where  $R_s \equiv c R_{200}$  is the scale radius and  $c$  is a dimensionless concentration parameter.

For the gas we use the KS model that derives from early hydrodynamical simulations (Komatsu & Seljak 2001),

$$\rho_{\text{KS}}(r) = \rho_0 \left( \frac{\ln \left( 1 + \frac{r}{R_s} \right)}{\frac{r}{R_s}} \right)^{1/\Gamma-1}, \quad (9)$$

where  $R_s$  is as defined in the NFW model,  $\rho_0$  is the central density parameter, and  $\Gamma$  is the polytropic index of the gas, which defines the gas' equation of state,  $P_{\text{gas}} \propto \rho_{\text{gas}}^{\Gamma}$ , where  $P_{\text{gas}}$  is the gas pressure and  $\rho_{\text{gas}}$  is the gas density.

For 2D profile fitting, the above models are projected according to

$$\Sigma(r) = 2 \int_0^{\sqrt{r_{200}^2 - r^2}} \rho(\sqrt{r^2 + z^2}) dz, \quad (10)$$

where the upper limit of integration is not  $\infty$  because we only measure profiles for particles within  $r_{200}$  (in 2D and 3D).

For the NFW fits, we take  $c$  and  $R_s$  as the free parameters. For the KS fits, we first fit the corresponding dark matter only profile to the NFW model to get  $R_s$ , then we fit the gas profile to the KS model with  $\rho_0$  and  $\Gamma$  as free parameters. The reduced  $\chi^2$  values for each fit are also tracked as a measure of goodness-of-fit. Once the best-fitting parameters are determined, we calculate the mass bias for each mass bin and centroid definition (Table 1), defined as

$$\text{Mass bias} \equiv \left( \frac{M_{200}^{\text{fit}}}{M_{200}^{\text{MBP}}} - 1 \right) \times 100, \quad (11)$$

where  $M_{200}^{\text{fit}}$  is

$$M_{200}^{\text{fit}} \equiv \int_0^{r_{200}} \rho(r|\{p_{\text{best fit}}\}) 4\pi r^2 dr. \quad (12)$$

Here  $\{p_{\text{best fit}}\}$  is the set of best-fitting parameters: for the all-particle case it is  $\{\rho_0, c, R_s\}$ , while for the gas-only case it is  $\{R_s, \rho_0, \Gamma\}$ . Note that for the 2D analysis,  $M_{200, \text{fit}}$  is obtained from the 3D profile,  $\rho(r)$ , but with profile parameters that are fit to the 2D data,  $\Sigma(r)$ . The ‘true’ value,  $M_{200}^{\text{MBP}}$ , is measured by directly summing the masses of all particles within  $r_{200}$  of the MBP. In order to estimate uncertainties in the fit parameters, we bootstrap resample clusters in each mass bin 20 times, with replacement. Each time we stack and fit for the model parameters, evaluate  $\chi^2$ , and measure the mass bias. The uncertainties are given by the standard deviation of the resampled estimates.

#### 4.2 Centred fit analysis

To establish a baseline, we first conduct a profile analysis relative to the ‘true’ centre, the MBP. The 3D and 2D profiles and fits are shown in Fig. 6. The stacked cluster profiles are not especially well described by the models, which is reflected in reduced  $\chi^2$  value of  $\sim 2\text{--}3$ , as shown in Fig. 7. This is due to the fact that the average density profiles are formed from clusters of different masses (within the mass bin). The discrepancy is resolved if we adopt the theorist perspective: individually fitting each cluster profile, then averaging the fit parameters within each mass bin. However, since we are trying to characterize the biases that result from stacking profiles, the mis-centred results presented below include the small bias due to stacking over a finite mass range.

In both the all-particle case (fit by the NFW model) and the gas case (fit by the KS model), the recovered mass is underestimated by a few per cent. As shown in the lower right-hand panels of Fig. 7 (blue curves), the bias is largest for the lighter clusters, and approaches zero for the most massive clusters.

#### 4.3 Mis-centred fit analysis

The best-fitting profile parameters for each centroid definition in Table 1 are shown in Figs 7 and 8. The results are plotted as a function of the true cluster mass,  $M_{200}$ , measured with respect to the MBP. For each case (NFW and KS), the upper panels show the best-fitting model parameters, while the bottom panels show the reduced  $\chi^2$  for each fit along with the inferred mass bias. Uncertainties are estimated using bootstrap resampling.

For the NFW profiles, the three gas-based centroids generally yield small mass biases of  $< \sim 5$  per cent, in accord with their small offsets. The SCOM-centred profiles fit badly but the mass error ends up being relatively small. It appears that shifts in the fits of  $c$  and  $R_s$  (relative to the MBP-based values) compensate in the product  $R_{200} \equiv c R_s$ , leaving only a small bias in  $M_{200}$ . The SMGC- and SMGL-centred profiles produce mass biases of up to 10–20 per cent

in the 3D case but less than 10 per cent in 2D. The SITR-centred profiles produce a mass bias of  $\sim 6$  per cent in 3D, which agrees with our earlier observation that SITR is a marginally better galaxy-based centroid, comparing to SMGC and SMGL.

For the KS profiles, the MBP, SCOM, and the three gas-based centroids generally provide unbiased cluster masses but the SMGC and SMGL centroids produce a relatively large mass bias of  $\sim 10\text{--}15$  per cent in 3D and  $\sim 8$  per cent in 2D. The SITR-centred profiles give a slightly smaller mass bias than the SMGC and SMGL centroids, especially for high-mass clusters. Overall, there are no compelling trends as a function of the true cluster mass.

As a final note, we explore the degree to which stacking itself, rather than mis-centring, is contributing to bias in the inferred parameters. To do so, we measure and fit the density profiles for each cluster, then calculate the mean and standard deviation of the best-fitting model parameters within a mass bin. The reduced  $\chi^2$  is significantly closer to 1, in agreement with the MBP-based results in Section 4.2. However, the average best-fitting model parameters and inferred mass biases are not significantly different from the results of fitting to the stacked profiles. We conclude that the biases shown in Figs 7 and 8 are indeed due to centroid offsets.

## 5 CONCLUSIONS

Using catalogues derived from the BAHAMAS hydrodynamical simulations, we investigate seven observationally motivated cluster centroid definitions (Table 1). These include: SITR, SCOM, SMGC, SMGL, GSXP, GBXP, and GCYP.

We first evaluate the distribution of offsets that these centroids possess, relative to the MBP in the cluster (defined to be the ‘true’ centre). We characterize the offsets in 2D and 3D using an analytical parametrization. Our model divides the clusters into two groups: a ‘well-centred’ group described by an Exponential distribution and a ‘mis-centred’ group described by Gamma distribution. The E $\Gamma$  model fits generally well to the offset distributions. The parameters for this offset model appear in Fig. 4. The results are in agreement with Cawthon et al. (2018). Future studies of cluster density profiles could use this description to characterize mis-centred profiles.

The best-fitting models in Fig. 4 show that the gas-based centroids GSXP, GBXP, and GCYP have the smallest average offsets, as illustrated in Fig. 3. The SITR, SMGC, and SMGL centroids are clearly divided into a well-centred group and mis-centred group. About 60 per cent of these centroids are well-centred, consistent with the findings of Cawthon et al. (2018) and Cibirka et al. (2017). However, our analysis differs in that Cawthon et al. (2018) do not use the MBP as the true centre and have a much smaller cluster sample size, while Cibirka et al. (2017) use only the Rayleigh distribution to describe the mis-centred group. SCOM does not have a distinct well-centred group, however, the scatter of the mis-centred group is smaller than that of the mis-centred SITR, SMGC, and SMGL groups. Based on this, we conclude that SITR is the best galaxy-based centroid, in agreement with Robotham et al. (2011). There is no discernible relation between centroid offset and cluster mass for the galaxy-based centroids (Fig. 5), however, the gas-based centroid offsets generally decrease with increasing cluster mass until  $\sim 10^{14.4} M_{\odot}$ , above which the offsets increase for the largest mass clusters (possibly due to recent major mergers).

We study stacked cluster density profiles using (i) all the particles, and (ii) only the gas particles, in both 2D and 3D, centring each on the MBP and then on seven observationally motivated centroids. We stack and average the density profiles in each of 20 mass bins and fit them with empirical models. The reduced

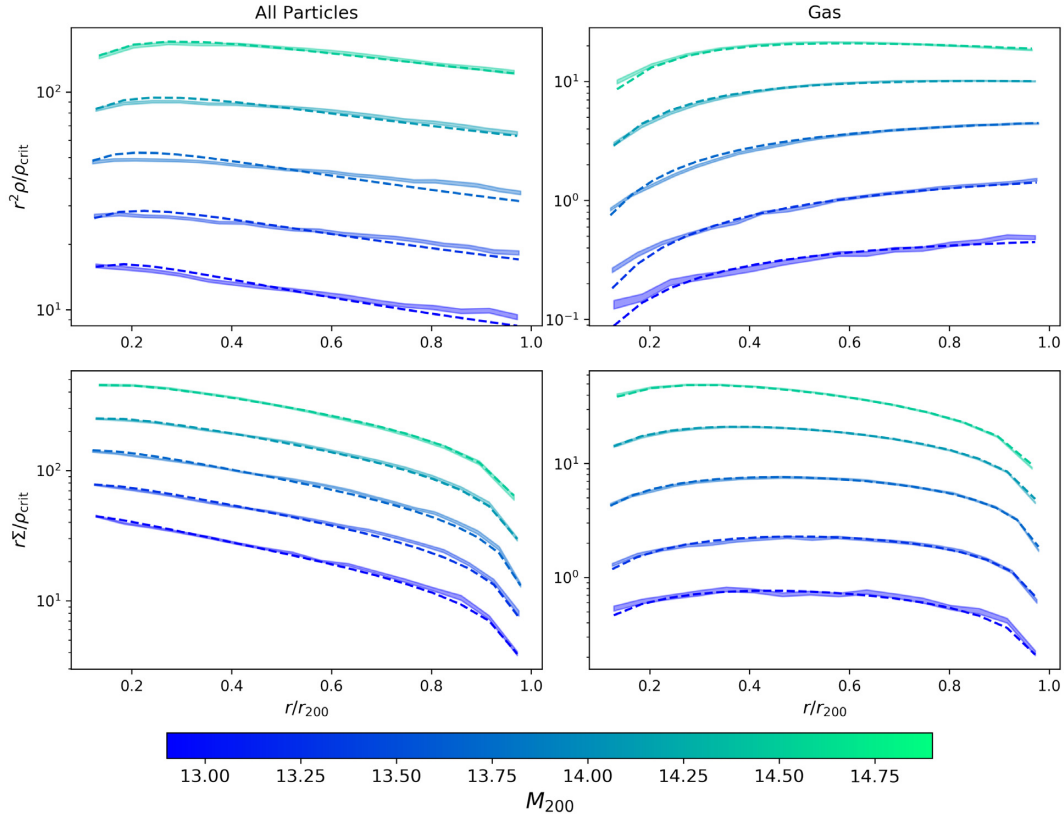


**Figure 6.** Stacked cluster density profiles, centred on the MBP (the true centre). The left-hand panels show the all-particle profiles along with the best-fitting NFW profiles (dashed); the right-hand panels show the gas density profiles, along with the best-fitting KS profiles (dashed). Upper panels show the 3D profiles, while the lower panels show the 2D surface density profiles. Different colours correspond to different mass bins (only a selection of mass bins is shown.) The small model errors due to stacking produce a small mass bias, as shown in Fig. 7.

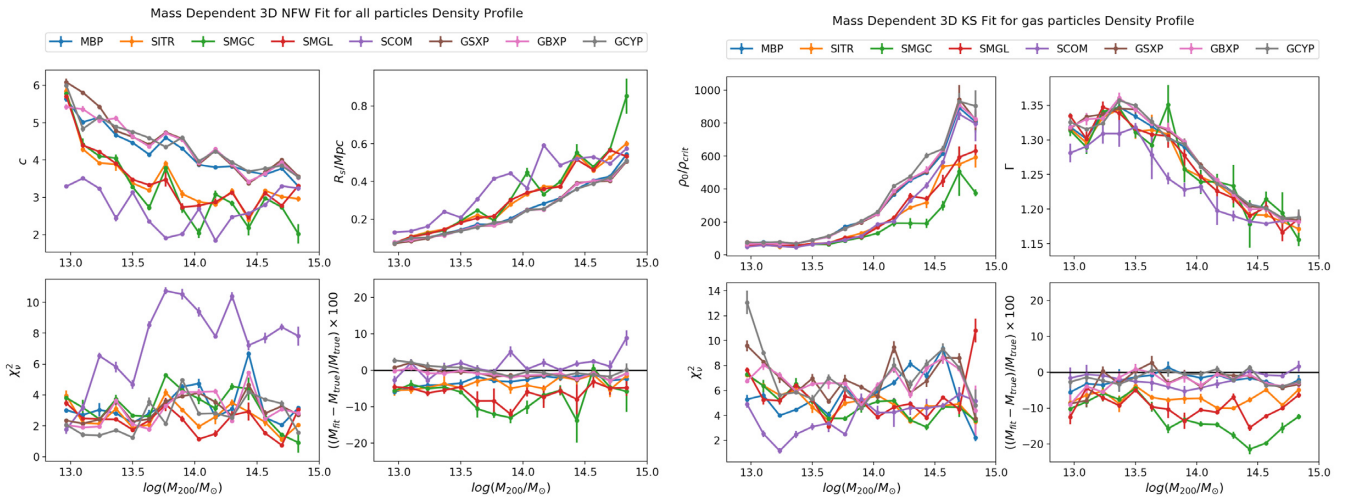


**Figure 7.** Left-hand panels: NFW model parameters fit to the 3D all-particle density profiles. Right-hand panels: KS model parameters fit to the 3D gas density profiles. For each case, the upper panels show the best-fitting model parameters, while the lower panels show the reduced  $\chi^2$  of each fit and the inferred mass bias.

$\chi^2$  values are generally greater than one, indicating that stacked profiles are not especially well fit by single-cluster models. This is improved when we measure and fit density profiles individually. The mass bias inferred from fitting NFW profiles to the all-particle

profiles typically underestimate the true mass by  $\sim 5$  per cent for most centroids. But the 3D profiles centred at SMGC and SMGL underestimate cluster mass by  $\sim 10$  per cent, and thus are even more biased. For the gas density profiles, the reduced  $\chi^2$  values do not

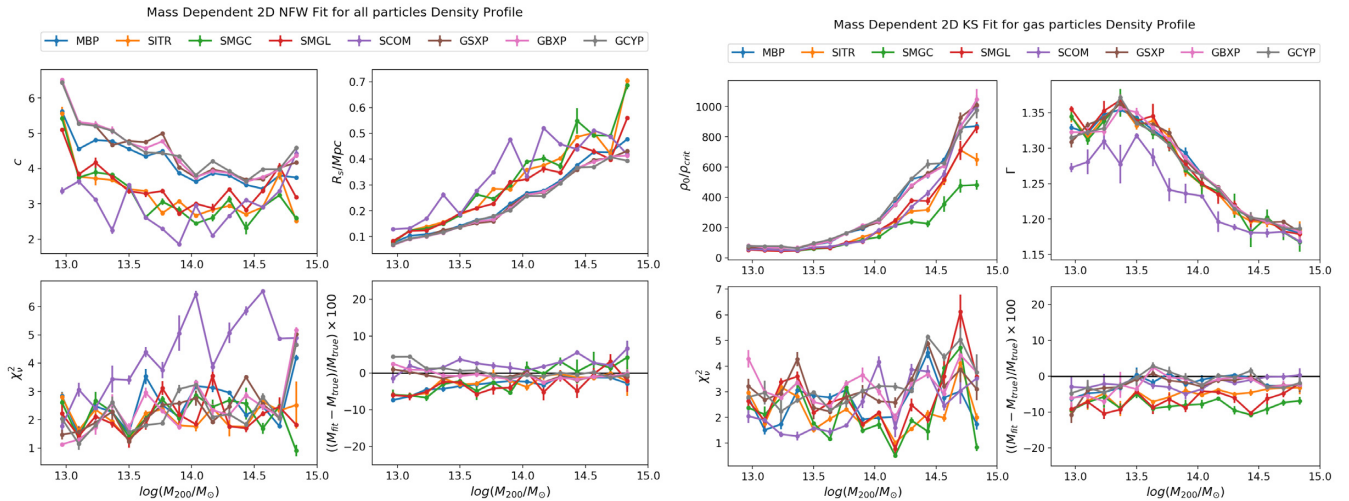


**Figure 8.** Left-hand panels: NFW model parameters fit to the 2D all-particle density profiles. Right-hand panels: KS model parameters fit to the 2D gas density profiles. For each case, the upper panels show the best-fitting model parameters, while the lower panels show the reduced  $\chi^2$  of each fit and the inferred mass bias.

depend significantly on centroid choice while the cluster masses are again generally underestimated by about 5 per cent, with the SMGC and SMGL centroids again performing more poorly.

Future observational studies of galaxy cluster masses and shapes should account for the fact that cluster mis-centring can bias the inference of cluster mass from stacked data. Particularly galaxy-based centroid definitions have a significant mis-centred population whose offsets from the true centre (the MBP) are larger than the gas-based centroid definitions. In any case, we present a model for the mis-centring PDF that will allow future researchers to convolve theoretical profile models with this PDF to account for the effects of mis-centring. It may also be fruitful to use a combination of the different centroid definitions to determine the position of the true centre (MBP) more accurately (beyond the scope of this paper).

*Author Contributions:* N. Raza and Z. Yan contributed equally to this work.

## ACKNOWLEDGEMENTS

This work is financially supported by University of British Columbia, Canada’s NSERC, and CIFAR. AJM and TT have received funding from the European Union’s Horizon 2020 research and innovation programme under the Marie Skłodowska-Curie grant agreements No. 702971 (AJM) and No. 797794 (TT).

## REFERENCES

- Andreon S., 2015, *A&A*, 582, A100  
 Borgani S., Kravtsov A., 2011, *Adv. Sci. Lett.*, 4, 204  
 Cawthon R. et al., 2018, *MNRAS*, 481, 2427  
 Cibirka N. et al., 2017, *MNRAS*, 468, 1092  
 Ford J. et al., 2015, *MNRAS*, 447, 1304  
 George M. R. et al., 2012, *ApJ*, 757, 2  
 Hinshaw G. et al., 2013, *ApJS*, 208, 19  
 Komatsu E., Seljak U., 2001, *MNRAS*, 327, 1353  
 Łokas E. L., Mamon G. A., 2001, *MNRAS*, 321, 155  
 McCarthy I. G., Schaye J., Bird S., Le Brun A. M. C., 2017, *MNRAS*, 465, 2936  
 McCarthy I. G., Bird S., Schaye J., Harnois-Deraps J., Font A. S., van Waerbeke L., 2018, *MNRAS*, 476, 2999

- Mantz A., Allen S. W., Rapetti D., Ebeling H., 2010, *MNRAS*, 406, 1759  
 Mantz A. et al., 2019, *BAAS*, 51, 279  
 Mihos Chris, 2003, preprint ([astro-ph/0305512](https://arxiv.org/abs/astro-ph/0305512))  
 Navarro J. F., Frenk C. S., White S. D. M., 1997, *ApJ*, 490, 493  
 Robotham A. S. G. et al., 2011, *MNRAS*, 416, 2640  
 Schaye J. et al., 2010, *MNRAS*, 402, 1536  
 Schrabback T. et al., 2018, *MNRAS*, 474, 2635  
 Simionescu A. et al., 2019, *Space Sci. Rev.*, 215, 24  
 Walker S. et al., 2019, *Space Sci. Rev.*, 215, 7  
 Zhang Y. et al., 2019, *MNRAS*, 487, 2578

## APPENDIX A: OTHER OFFSET PDF MODELS

In general, the PDF of centroid offset can be written as

$$P_M(r|f, \sigma, \tau) = f P_1(r|\sigma) + (1 - f) P_2(r|\tau), \quad (\text{A1})$$

where  $P_1(r|\sigma)$  describes the centred population and  $P_2(r|\tau)$  describes the mis-centred population. As shown in Table A1, we explore five additional combinations of Gamma, Rayleigh, Gaussian, and exponential distributions for  $P_1$  and  $P_2$  in addition to the  $E\Gamma$  model used in the main text.  $\sigma$  and  $\tau$  are the width parameters of the two distributions, and  $f \in [0, 1]$  is the fraction of clusters that

**Table A1.** The models we use to fit the offset distribution. In the abbreviations, ‘E’ stands for the exponential distribution; ‘ $\Gamma$ ’ for the Gamma distribution with shape parameter  $k = 2$ ; ‘R’ for the Rayleigh distribution, and ‘G’ for the Gaussian distribution.

Name	$P_1(r \sigma)$	$P_2(r \tau)$
$\Gamma\Gamma$	$\frac{r}{\sigma^2} \exp(-\frac{r}{\sigma})$	$\frac{r}{\tau^2} \exp(-\frac{r}{\tau})$
GG	$\frac{4\pi r^2}{\sigma^3(2\pi)^{3/2}} \exp(-\frac{r^2}{2\sigma^2})$	$\frac{4\pi r^2}{\tau^3(2\pi)^{3/2}} r^2 \exp(-\frac{r^2}{2\tau^2})$
RR	$\frac{r}{\sigma^2} \exp(-\frac{r^2}{2\sigma^2})$	$\frac{r}{\tau^2} \exp(-\frac{r^2}{2\tau^2})$
$E\Gamma$	$\frac{1}{\sigma} \exp(-\frac{r}{\sigma})$	$\frac{r}{\tau} \exp(-\frac{r}{\tau})$
EG	$\frac{1}{\sigma} \exp(-\frac{r}{\sigma})$	$\frac{4\pi r^2}{\tau^3(2\pi)^{3/2}} r^2 \exp(-\frac{r^2}{2\tau^2})$
ER	$\frac{1}{\sigma} \exp(-\frac{r}{\sigma})$	$\frac{r}{\tau^2} \exp(-\frac{r^2}{2\tau^2})$

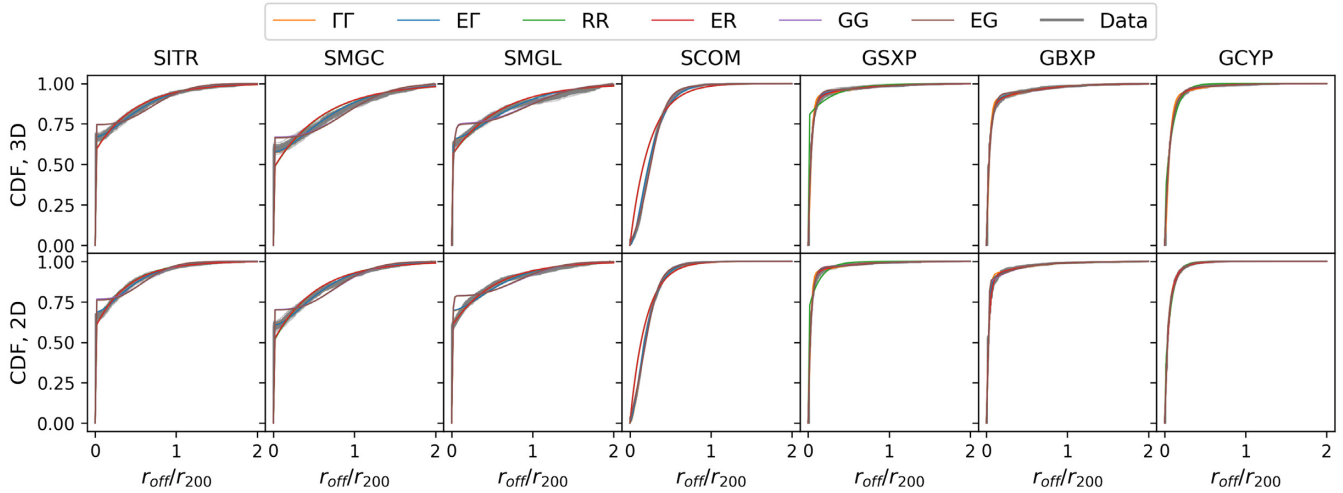


**Figure A1.** The measured (grey) and six fitted models (as defined in Table A1) of offset CDF from the MBP, for all seven centroids analysed. The upper panels show the 3D analysis, and the lower panels show the 2D analysis. The grey collection of lines is the results of all bootstrap resampled offset CDFs.

**Table A2.** Reduced  $\chi^2$  values, in 3D, for each PDF model defined in Table A1 and centroid defined in Table 1.

	SITR	SMGC	SMGL	SCOM	GSXP	GBXP	GCYP
$\Gamma\Gamma$	1.07	8.17	12.11	5.49	3.2	2.92	4.1
$E\Gamma$	1.09	6.82	10.8	5.33	1.05	0.9	0.72
RR	5.46	21.18	18.72	100.58	18.37	0.46	10.31
ER	6.04	19.8	16.66	98.19	0.57	0.47	0.73
GG	11.77	10.74	16.45	2.86	2.64	4.09	1.14
EG	13.74	10.93	16.2	2.82	2.85	3.96	1.22

**Table A3.** Reduced  $\chi^2$  values, in 2D, for each PDF model defined in Table A1 and centroid defined in Table 1.

	SITR	SMGC	SMGL	SCOM	GSXP	GBXP	GCYP
$\Gamma\Gamma$	1.36	2.43	6.82	1.27	4.13	4.01	3.16
$E\Gamma$	1.2	2.56	6.89	1.1	1.58	3.18	2.24
RR	2.44	8.37	4.64	39.34	16.12	1.04	0.87
ER	2.88	9.54	5.68	40.15	0.96	1.08	0.97
GG	14.91	13.41	19.66	2.45	3.16	7.27	3.73
EG	15.12	13.72	20.97	2.34	3.14	7.38	3.81

belong to the centred population.

The fitting procedure is exactly the same as Section 3.1. The best-fit CDF models are presented in Fig. A1. To compare the goodness-of-fit for the different models, we calculate the reduced  $\chi^2$ ,

$$\frac{\chi^2}{\text{d.o.f}} = \frac{1}{N_{\text{bin}} - 3} \sum_{i,j} [C_M(r_{\text{off},i}|f, \sigma, \tau) - C_D(r_{\text{off},i})]^T \times \text{Cov}^{-1}(r_{\text{off},i}, r_{\text{off},j}) [C_M(r_{\text{off},j}|f, \sigma, \tau) - C_D(r_{\text{off},j})],$$

where  $C_D$  is the measured offset distribution,  $C_M$  is the fitted CDF model, and  $\text{Cov}$  is the covariance matrix of  $C_D$ . The number of bins is  $N_{\text{bin}} = 20$ , while the number of degrees of freedom is  $N_{\text{bin}} - 3 = 17$ . The resulting  $\chi^2$  values are listed in Tables A2 and A3.

Surveying across all the values from both tables, we see that the  $E\Gamma$  model (see Table A1) generally provides the best description of the various centroid distributions, since it consistently produces one of the lowest (if not *the* lowest) reduced  $\chi^2$  values for all centroid definitions.

This paper has been typeset from a  $\text{\TeX}/\text{\LaTeX}$  file prepared by the author.